Chapter III

In situ structure of the complete *Treponema primitia* flagellar motor

Gavin E. Murphy[1], Jared R. Leadbetter[2], Grant J. Jensen[1*]

Divisions of Biology[1] and Environmental Science and Engineering[2]

California Institute of Technology, Pasadena, CA 91125

*To whom correspondence should be addressed: 1200 E. California Blvd., Pasadena, CA 91125, 626-395-8827 (phone), 626-395-5730 (fax), Jensen@caltech.edu.

Published in Nature 2006 Aug 31; 442 (7106): 1062-4.

doi:10.1038/nature05015

Received 7 April 2006; Accepted 21 June 2006; Published online: 2 August 2006

http://www.nature.com/nature/journal/v442/n7106/full/nature05015.html

The bacterial flagellar motor is an amazing nanomachine: built from about 25 different proteins, it uses an electrochemical ion gradient to drive rotation at speeds of up to 300 Hz[1, 2]. The flagellar motor consists of a fixed, membrane-embedded, torque-generating stator and a typically bidirectional, spinning rotor that changes direction in response to chemotactic signals. While most structural work to date has targeted the purified rotor[3, 4], little is known about the stator and its interactions. Using electron cryotomography of whole cells, here we show the *in situ* structure of the complete flagellar motor from the spirochete *Treponema primitia* at 7 nm resolution. Twenty individual motor particles were computationally extracted from the reconstructions, aligned, and then averaged. The stator assembly, revealed for the first time, possessed 16-fold symmetry and was connected directly to the rotor, C ring, and a novel P-ring-like structure. The unusually large size of the motor suggested mechanisms for increasing torque and supported models wherein critical interactions occur atop the C ring, where our data suggest that both the C-terminal and middle domains of FliG are found.

The bacterial flagellar motor excites considerable interest because of the ordered expression of its genes, its regulated self-assembly, the complex interactions of its many proteins, and its startling mechanical abilities. Stator proteins MotA and MotB form a ring of "studs" within and above the inner membrane that couple the passage of protons across the membrane to the generation of torque[1, 2]. Above the membrane MotB has a peptidoglycan-binding domain that presumably holds the stator in place by binding to the globally cross-linked peptidoglycan layer[1, 2]. Below the membrane, the cytoplasmic loops of MotA are believed to spin a wheel of FliG molecules, which, like radial spokes, extend roughly parallel to the membrane from the rotor in the middle to just below MotA on the periphery[1]. Proteinaceous P and L rings serve as bearings to facilitate the rotation of the rod within the peptidoglycan and outer membranes, respectively[1, 2]. Inside the cell

and below FliG lies the C ring, which regulates the direction of rotation in response to the chemotactic system[1, 2].

Flagellar basal bodies containing the rotor, rod, and sometimes the C ring have been purified and reconstructed by electron cryomicroscopy-based single particle analysis[3, 5, 6]. The *Salmonella* rotor possessed 26-fold symmetry[7] while the *Salmonella* C ring possessed a mean symmetry of 34[8]. Because the stators do not co-purify with the rotor, however, little is known about their structure and interactions with the rest of the motor. Patterns of stator studs have been seen in 2D, freeze-etch images, but the interpretation of these images is difficult and the number of studs has been reported as either 12 or 16, depending on the species[9-12]. 2-D cryo-EM images of purified PomA/PomB complexes (homologs of MotA and MotB) from *V. alginolyticus* have revealed an ~ 70 Å long, thin extension above the membrane[13].

Here we report the complete structure of the flagellar motor, including the stators, obtained by electron cryotomography. Fifteen *T. primitia* cells frozen within thin layers of vitreous ice were imaged (Fig. III-1a, and Methods section). *T. primitia* was chosen for its narrow diameter and interesting periplasmic flagella that emerge from each pole. Twenty motor particles were computationally extracted from the reconstructions, mutually aligned, and averaged (Figures III-1b–e). In both individual maps (Fig. III-1d) and their average (Fig. III-1e), the stator studs were clearly sixteen-fold symmetric around the rod. We checked for symmetry computationally in the other components including the P-collar (the density above the stator as explained below), the rotor, the connections between the stators and C ring, and the C ring itself (Supplementary Fig. III-S1a and b). Presumably because of the limited resolution, only the symmetry of the stators and their connections to the C ring was apparent. This symmetry was therefore

imposed on the entire motor, effectively smoothing the other components (Supp. Fig. III-S1c and d).

For the first time, the 3-D structure of the stators was revealed in their natural position in contact with the membrane and other motor components (Fig. III-2 and Supplementary Movie). The 16 stator studs (two of which are identified by asterisks in Fig. III-2c) were 8 nm wide, which is similar to the reported values of 5–7 nm seen by other means[9, 10, 12]. Surprisingly, the volume of each stud above the membrane was ~ 20 times larger than that expected for two MotB peptidoglycan binding domains and much thicker than PomA/PomB resuspended in liposomes[13]. The identity of the rest of the stator density is unclear. The studs were spaced 7 nm apart, which is sufficient to accommodate hypothetical models for the 18 transmembrane helices in a $MotA_4MotB_2$ torque-generating unit[14]. The average stud was not vertical—instead, it leaned (dotted line in Fig. III-2a) such that its distal end was positioned clockwise relative to the proximal end as viewed from inside the cell. There were thin bridging densities connecting the stud heads around the ring (arrowhead in Fig. III-2c).

Four bridging densities (numbered in Fig. III-2b) were seen connecting the stator ("S" in Fig. III-2b) to other components of the motor (see Supp. Fig. III-S2 for contour, variance, and statistical significance maps). Bridging density #1 connected the stator to the C ring ("C" in Fig. III-2b). It is thought that a series of charged residues in a cytoplasmic loop of MotA interacts here with complementary charges in the C-terminal domain of FliG[1]. The stator-C-ring connections were also rotated with respect to the periplasmic studs, suggesting that they might perhaps be the terminus of a ~ 24 nm long and straight component that extended from the peptidoglycan layer all the way through the membrane to the C ring (see again dotted line in Fig. III-2a). Bridging densities #2 and #3 were finger-like extensions connecting the stator directly to the rotor.

Bridging density #4 linked the stator to a contrast-rich ring of density ("P" in Fig. III-2b) encircling the rod above the rotor reminiscent of the P- and L-ring bushings in *Salmonella* and *E. coli*. Sequenced *Treponema* flagellar proteins are similar to the better known *Salmonella* and *E. coli* versions (see Supplementary Data), except that the genes for the P and L ring proteins FlgI and FlgH are missing[15]. The absence of an L-ring is understandable because *Treponema*'s periplasmic flagella never exit the outer membrane, and not surprisingly, isolated *Treponema* basal bodies lack any ring structures[16]. In our *in situ* reconstructions, however, an additional ring was seen just above the stators at the level of the peptidoglycan layer, but ~ 8 nm away (surface to surface) from the rod itself. We therefore refer to it as the "P-collar" to reflect its position and loose fit around the rod, though the gene responsible for this density is unknown. This structure may serve to limit the tilt of the flagellar hook and may also further stabilize the stators.

The rotor itself ("R" in Fig. III-2b) was bowl-shaped. Unlike previous work on the isolated basal body, in which the membrane location was not certain[3, 7], here the bulk of the rotor was seen to lie just beneath the inner membrane ("IM" in Fig. III-2b) submerged within the C ring. At the bottom of the rotor there was a small ring (arrow in Fig. III-2d) that formed a funnel-like pore, which may perhaps be the insertion apparatus through which flagellin monomers are exported. Another contrast-rich density with low variance (See Supplementary Figure III-S2) was visible 4 nm below the pore and because of its proximity, has been labeled an export bundle ("E" in Fig. III-2b).

In comparison to isolated *Salmonella* basal bodies, which have been reconstructed to higher resolution by single particle analysis[3, 5], the *Treponema* stud ring, C ring, and rotor are all much larger (Fig. III-3). The rotor is also located lower within the C ring and appears bowl-shaped rather than disk-like. Interestingly, by stereo-photogrammetry the *Salmonella* rotor also appeared bowl-shaped *in situ*[17], so the shape may depend on

conditions lost during purification. The *Caulobacter* rotor has also appeared bowl-shaped in some reconstructions[6]. Other structural details are remarkably conserved, such as the small gap between rotor and rod (arrows in Fig. III-3c and III-3d).

These differences have important implications for current models of the functional and architectural relationships of the components. While the *Salmonella* motor spins just the flagellum, because *Treponema* flagella are periplasmic, it is thought that they cause the whole cell to gyrate[18]. Thus each rotation may be much slower and require greater torque. The unusually large stud ring, C ring, and rotor in *Treponema* may serve to increase torque by increasing the length of the effective lever arm through which each stator stud acts. These larger rings may also accommodate more stator studs and FliG molecules around the ring, in effect "gearing down" the *Treponema* motor so that the passage of each proton across the membrane produces a smaller angular rotation.

FliG is thought to have three domains: a C-terminal domain directly underneath the stator that forms the top of the C ring, a middle-domain whose location is uncertain, and an N-terminal region bound to the rotor[1, 2, 4, 19, 20]. In our reconstructions, the stator-C-ring connection appears on the outside edge of the C ring, and the distance between the C ring and the rotor is too large to be spanned by the 2 nm long alpha helix connecting FliG's C-terminal and middle domains (see Supplementary Data and starred gap in Fig. III-3). The simplest interpretation of these results is that the C-terminal domain forms the outside edge of the C ring; both the C-terminal and middle domains of FliG lie atop the C ring, and a portion of the N-terminus acts as an extended tether spanning the gap to the rotor, as argued elsewhere[19, 20]. It is interesting to note that while the diameters of the stud and C rings in *Treponema* are unusually large, nevertheless they still match, so that the studs appear directly above the C ring. The available data suggest that the same relationship holds in other, smaller motors as well [3, 11], supporting the idea that this

juxtaposition is important and that key functional interactions do indeed occur at this interface.

Methods

Exponential phase cultures of *T. primitia* strain ZAS-2[21] were plunge frozen with gold fiducial markers across EM grids in liquid ethane. *T. primitia* is an obligate anaerobe but can tolerate atmospheric conditions for about 20 minutes, so grids were frozen quickly in small batches. Single-axis tilt series were acquired automatically on a 300 keV FEI Polara FEG TEM. The 20 averaged motors were taken from tilt-series with underfocuses between 10 and 18 μm (first CTF zero between 4.5 and 6.0 nm^{-1}). Tomograms were low-pass filtered at the resolution of the first CTF zero and binned once (1.96 nm/pixel). No other CTF corrections were performed.

Twenty motor particles were computationally extracted from the tomograms and aligned to an arbitrarily chosen reference particle. The aligned motors were then averaged and rotated so the rod axis corresponded to the z-axis. To detect the symmetry of the components, annular masks were generated for the five different motor regions (shown in Supp. Fig. III-S1b), and then applied separately to all twenty individual particles. The only detectable symmetry in the rotational power spectrum (16-fold) was found in the two stator regions (periplasmic and cytoplasmic), so this was applied to the entire averaged motor. This initial symmetrized average was used as a reference for a further alignment, and the process was iterated a total of five times. To test potential reference bias, two alternate particles were used as a reference, and the resulting average was essentially identical. A resolution of 7 nm was estimated by separately averaging and symmetrizing two halves of the data set and correlating them using Fourier shell correlation with a threshold of 0.5. The isosurface was contoured at a level that showed the connections between stator and C ring.

References

1. Kojima, S. & Blair, D. F. The bacterial flagellar motor: structure and function of a complex molecular machine. *Int. Rev. Cytol.* **233**, 93-134 (2004).

2. Berg, H. C. The rotary motor of bacterial flagella. *Annu. Rev. Biochem.* **72**, 19-54 (2003).

3. Francis, N. R., Sosinsky, G. E., Thomas, D. & DeRosier, D. J. Isolation, characterization and structure of bacterial flagellar motors containing the switch complex. *J. Mol. Biol.* **235**, 1261-70 (1994).

4. Thomas, D., Morgan, D. G. & DeRosier, D. J. Structures of bacterial flagellar motors from two FliF-FliG gene fusion mutants. *J. Bacteriol.* **183**, 6404-12 (2001).

5. Sosinsky, G. E., Francis, N. R., Stallmeyer, M. J. & DeRosier, D. J. Substructure of the flagellar basal body of *Salmonella typhimurium*. *J. Mol. Biol.* **223**, 171-84 (1992).

6. Stallmeyer, M. J., Hahnenberger, K. M., Sosinsky, G. E., Shapiro, L. & DeRosier, D. J. Image reconstruction of the flagellar basal body of *Caulobacter crescentus*. *J. Mol. Biol.* **205**, 511-8 (1989).

7. Suzuki, H., Yonekura, K. & Namba, K. Structure of the rotor of the bacterial flagellar motor revealed by electron cryomicroscopy and single-particle image analysis. *J. Mol. Biol.* **337**, 105-13 (2004).

8. Young, H. S., Dang, H., Lai, Y., DeRosier, D. J. & Khan, S. Variable symmetry in *Salmonella typhimurium* flagellar motors. *Biophys. J.* **84**, 571-7 (2003).

9. Khan, S., Dapice, M. & Reese, T. S. Effects of mot gene expression on the structure of the flagellar motor. *J. Mol. Biol.* **202**, 575-84 (1988).

10. Khan, S., Ivey, D. M. & Krulwich, T. A. Membrane ultrastructure of alkaliphilic *Bacillus* species studied by rapid-freeze electron microscopy. *J. Bacteriol.* **174**, 5123-6 (1992).

11. Khan, S., Khan, I. H. & Reese, T. S. New structural features of the flagellar base in *Salmonella typhimurium* revealed by rapid-freeze electron microscopy. *J. Bacteriol.* **173**, 2888-96 (1991).

12. Coulton, J. W. & Murray, R. G. Cell envelope associations of *Aquaspirillum serpens* flagella. *J. Bacteriol.* **136**, 1037-49 (1978).

13. Yonekura, K. et al. Electron Cryomicroscopic Visualization of PomA/B Stator Units of the Sodium-driven Flagellar Motor in Liposomes. *J. Mol. Biol.* **357**, 73-81 (2006).

14. Braun, T. F., Al-Mawsawi, L. Q., Kojima, S. & Blair, D. F. Arrangement of core membrane segments in the MotA/MotB proton-channel complex of *Escherichia coli*. *Biochemistry* **43**, 35-45 (2004).

15. Limberger, R. J. The periplasmic flagellum of spirochetes. *J. Mol. Microbiol. Biotechnol.* **7**, 30-40 (2004).

16. Jackson, S. & Black, S. H. Ultrastructure of *Treponema pallidum* Nichols following lysis by physical and chemical methods. II. Axial filaments. *Arch. Mikrobiol.* **76**, 325-40 (1971).

17. Katayama, E., Shiraishi, T., Oosawa, K., Baba, N. & Aizawa, S. Geometry of the flagellar motor in the cytoplasmic membrane of *Salmonella typhimurium* as determined by stereo-photogrammetry of quick-freeze deep-etch replica images. *J. Mol. Biol.* **255**, 458-75 (1996).

18. Charon, N. W. & Goldstein, S. F. Genetics of motility and chemotaxis of a fascinating group of bacteria: the spirochetes. *Annu. Rev. Genet.* **36**, 47-73 (2002).

19. Brown, P. N., Hill, C. P. & Blair, D. F. Crystal structure of the middle and C-terminal domains of the flagellar rotor protein FliG. *EMBO J.* **21**, 3225-34 (2002).

20. Lowder, B. J., Duyvesteyn, M. D. & Blair, D. F. FliG subunit arrangement in the flagellar rotor probed by targeted cross-linking. *J. Bacteriol*. **187**, 5640-7 (2005).

21. Leadbetter, J. R., Schmidt, T. M., Graber, J. R. & Breznak, J. A. Acetogenesis from H2 plus CO2 by spirochetes from termite guts. *Science* **283**, 686-9 (1999).

Supplementary information is linked to online versions of the paper at www.nature.com/nature.

Acknowledgements We thank Eric Matson for growing the *T. primitia* cultures. This work was supported in part by NIH grants P01 GM66521 and R01 AI067548 to G.J.J., DOE grant DE-FG02-04ER63785 to G.J.J., a Searle Scholar Award to G.J.J., NSF grant DEB-0321753 to J.R.L., NIH graduate fellowship F31 EB 004179 to G.E.M. and gifts to Caltech from the Ralph M. Parsons Foundation, the Agouron Institute, and the Gordon and Betty Moore Foundation.

Author Contributions G.E.M. collected/analysed the data and drafted the text and figures; J.R.L. provided cells and discourse and G.J.J. guided the research and manuscript editing throughout.

Author Information The averaged and symmetrized structure has been deposited in the EM Data Bank (http://www.ebi.ac.uk/msd/index.html) with the accession code EMD-4663. Reprints and permissions information is available at npg.nature.com/reprintsandpermissions. Address correspondence to G.J.J. at jensen@caltech.edu.

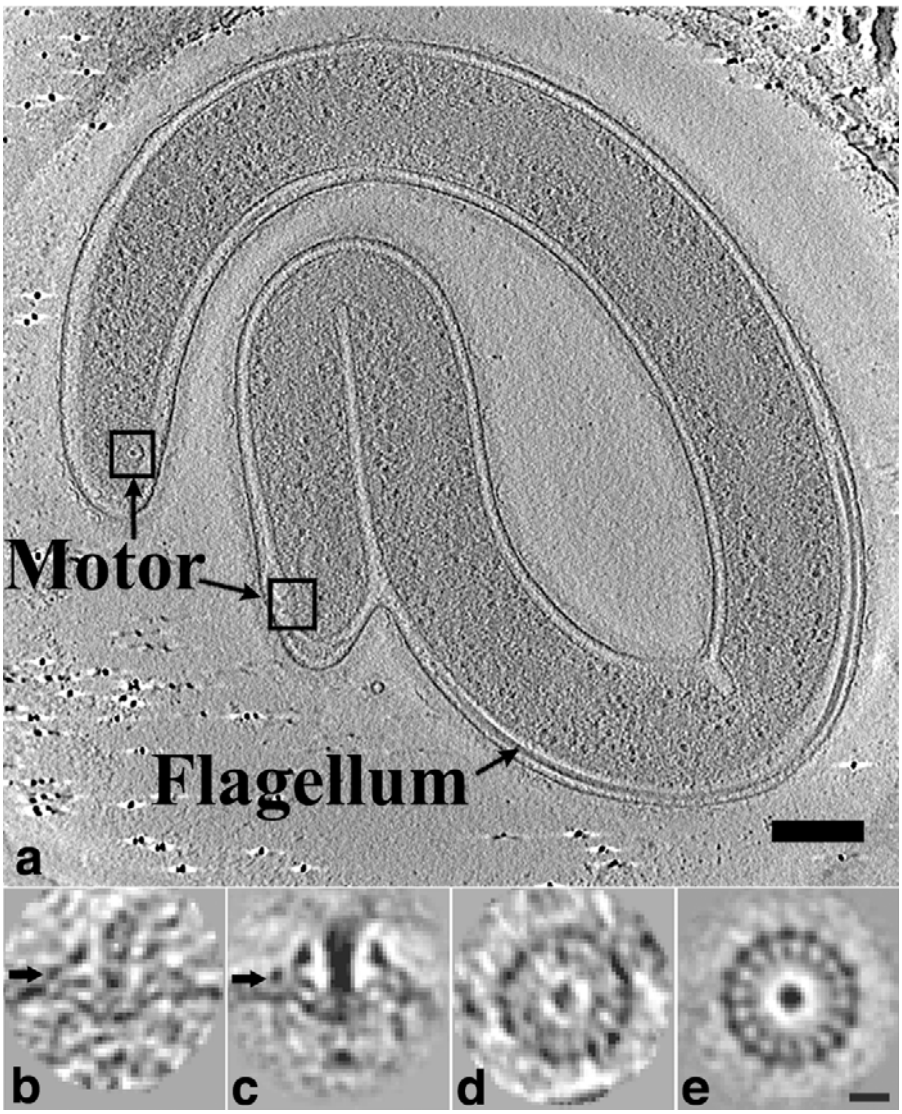

Figure III-1. Electron cryotomography of *T. primitia* and its periplasmic flagellar motor.

a) 2 nm thick central section through a tomogram of an entire *Treponema* cell. A flagellar motor is located near each cell tip and the flagella rotate in the periplasm (scale bar 200 nm). **b**) Axial slice through the center of one extracted motor particle. **c**) Axial slice through the average of twenty motor particles. **d**) Radial slice through the stator region of the same particle shown in **b**, taken at the

height indicated by the arrow. **e**) Radial slice through the average motor, taken at the height indicated by the arrow in **c** (scale bar 20 nm, for **b**-**e**).

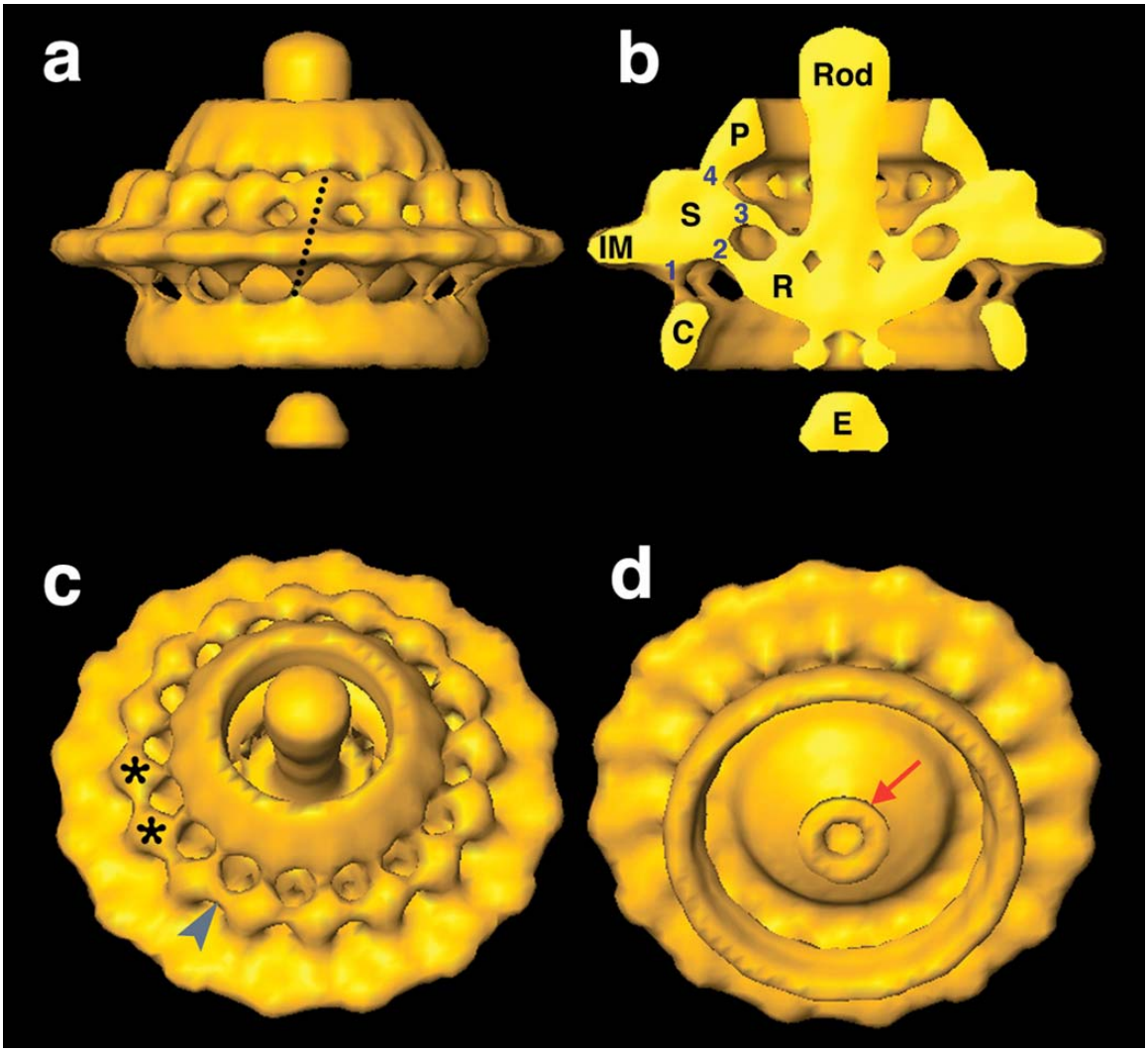

Figure III-2. Isosurface of the symmetrized average flagellar motor.

a) Side view. The dotted line indicates the tilt of the stators with respect to the membrane. **b**) Cutaway of the motor in the same orientation. The stators (S) are embedded in the inner-membrane (IM) and directly contact the C ring (C) (#1), the rotor (R) (#2 and #3) and the P-collar (P) (#4). A rod extends from the rotor, and a bundle (E) lies under the rotor's pore. **c**) Oblique view of the motor's top from within the periplasm. Note the arrangement of the stator studs (asterisks)

and their linkages (arrowhead). **d**) Oblique view of the motor's bottom from within the cytoplasm, with the bundle removed to reveal the pore ring (arrow).

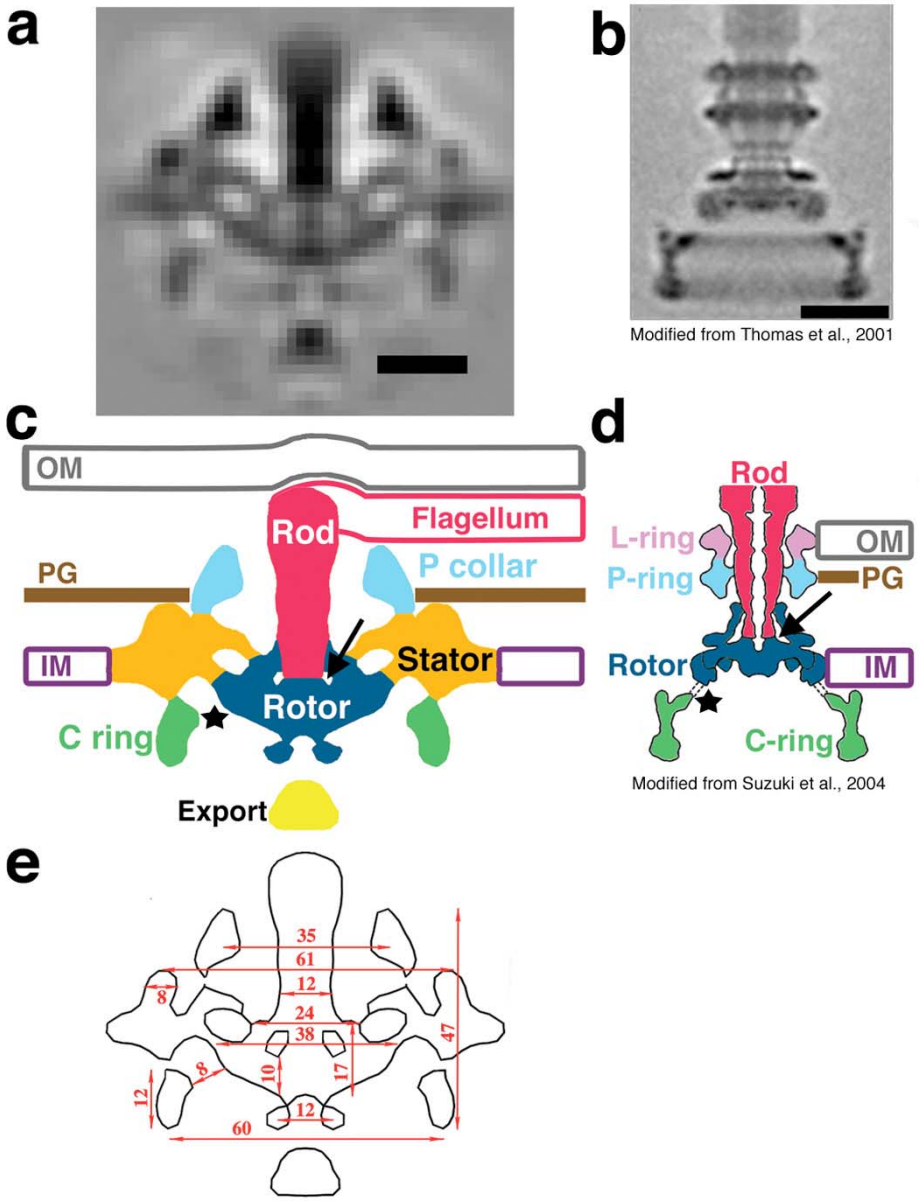

Figure III-3. The *Treponema* motor and its comparison to the *Salmonella* basal body.

All objects are at the same scale. **a**) Axial slice through the *Treponema* flagellar motor (scale bar 20 nm). **b**) Projection of the 3-D reconstruction of the *Salmonella* basal body (scale bar 20 nm). **c**) Cartoon interpretation of the *Treponema* motor with its components labeled. The arrows here and in panel **d**

point to the gap between the rotor and rod, while the stars indicate the gap between the C ring and rotor. The location of the peptidoglycan layer (PG) is conjectured. The outlined objects' locations are approximate. The flagellum actually bends more gradually over the P-collar in presumably random directions but appears straight when averaged. The inner membrane and outer membrane (OM) both bulge more widely around the motor *in situ* than is pictured. **d**) Cartoon of the *Salmonella* basal body for comparison. **e**) Measurements of various motor features.

Supplementary Information

Supplementary Figures

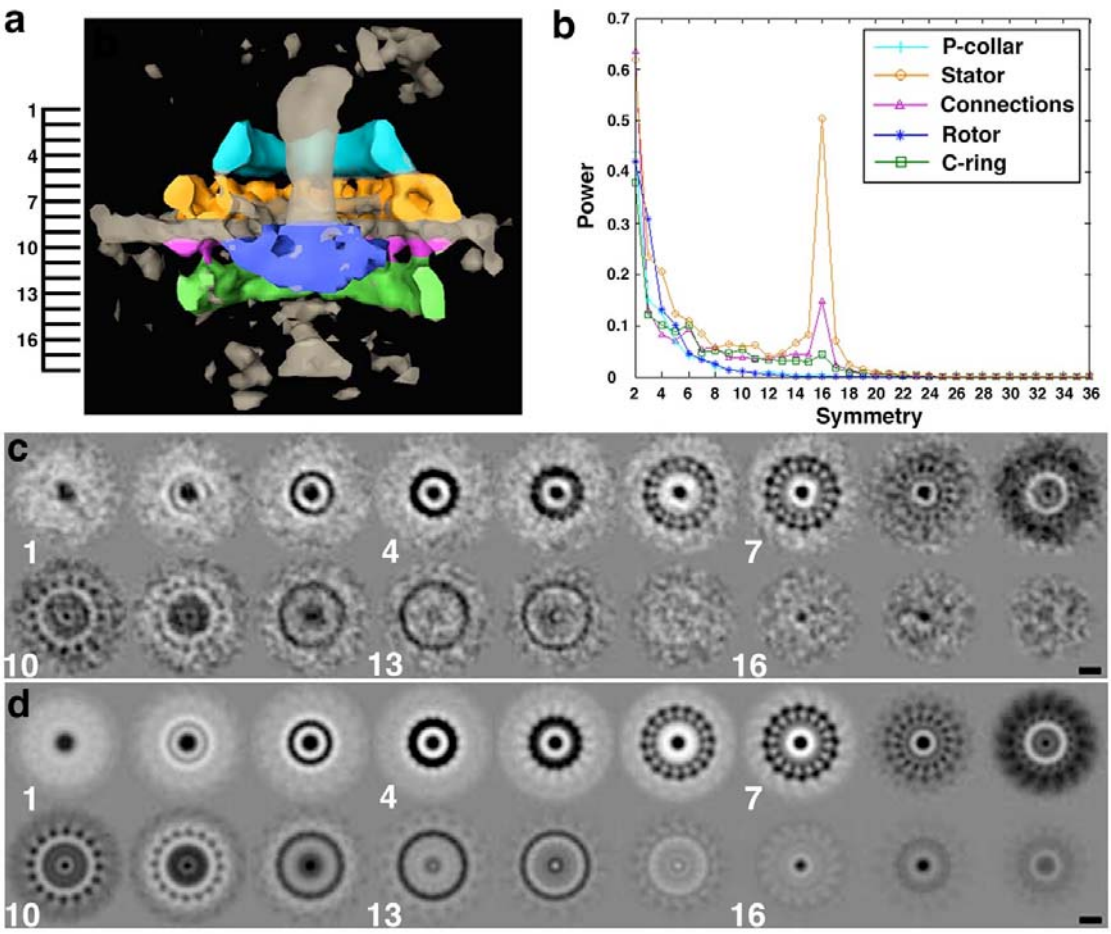

Figure III-S1. Symmetry of the motor components and 3.9-nm thick serial sections.

a) To detect the symmetry of the components in the average, annular masks were generated for the five different motor regions shown in the panel and then applied separately to all twenty individual particles. The regions that were not analyzed for symmetry are grey and transparent. The ruler on the left marks the heights of the radial sections shown in **c** and **d**. **b**) Rotational correlation coefficients were calculated by rotating each of the 100 objects (5 regions of 20 different motors) in 1° steps 360° around the z-axis and calculating the 3-D cross-correlation coefficient with the unrotated object.

The results were Fourier transformed in 1-D to produce rotational power spectra (one for each component of each motor), and then the average power spectrum for each component was plotted, as shown in the panel. The only symmetry detected was the 16-fold symmetry within the stator ring, so this symmetry was imposed on the entire motor, effectively smoothing the other components. **c)** Sections through the average motor. (Section 9 is through the membrane.) **d)** Sections through the symmetrized average. Note the symmetry of the stators both below (sections 10–11) and above (sections 6–8) the membrane (scale bar 20 nm, for **b** and **c**).

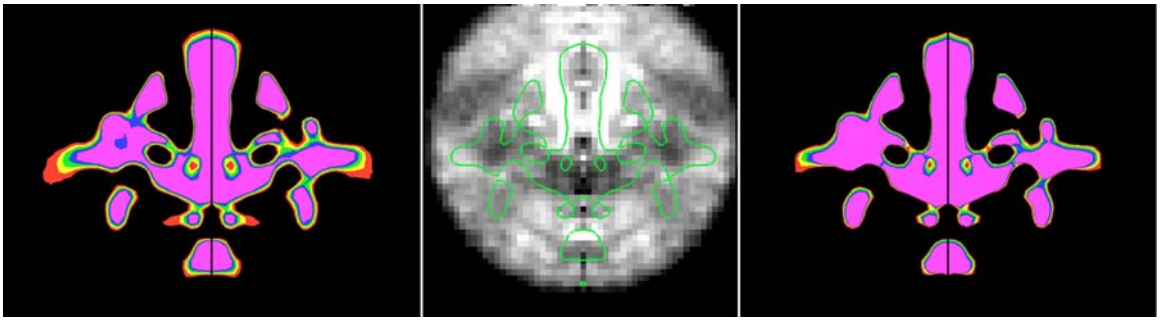

Figure III-S2. Significance maps.

a) An axial cutaway of the symmetrized average map contoured at various levels. Because the connections are not all coplanar, the left and right halves of the figure actually show different planes. The left half shows the plane that bisects connection #4 (see Fig. III-2 for numbering), while the right half bisects connection #1. The density threshold at which surface renderings of electron cryotomography maps should be contoured is usually unclear. The isosurfaces in Fig. III-2 correspond to 0.95 standard deviations above the mean. This value was chosen as the tightest contour that still manifests the connection between the stator assembly and the C ring known to exist from previous work[1]. Here four additional contours are shown as well. The colors red, yellow, green, blue and pink correspond to 0.45, 0.75, 0.95, 1.2, and 1.45 times the standard deviation, respectively. The steepest density gradients exist along the edges of the rod, while the most gradual occur at the edge of the stator assembly where the membranes of the individual motors continue outwards with somewhat variable curvature. The order of the connections in terms of density are, from largest to smallest, #2, #1 and #4, and finally #3. **b)** A 2 nm thick, axial section of the symmetrized variance map with the outline of the motor superimposed (at the favored, 0.95 standard deviation contour level, colored again in green). The highest variances occur around the

rod, as expected, since the rods in each individual motor emerge at different angles, bending over against the P-collar and underneath the outer membrane. The next highest variances are in the cytoplasm underneath the rotor. Some variance is seen in the regions of the connections, as well as on the top face of the export bundle. The rotor and stator stud regions of the map have the least variance. **c)** An axial cutaway of a symmetrized significance map, generated by subtracting from the normally distributed average map the product of 2.093 times the standard error map, which corresponds to the lower boundary of the "95% confidence" interval of a two-tailed student t-test for a sample size of 20[22]. The colors red, yellow, green, blue, and pink correspond to thresholds of 0.31, 0.41, 0.51, 0.61, and 0.71 times this map's standard deviation, respectively. The middle threshold (0.51, green) was chosen to again enclose the same favored volume as the isosurface in Fig. III-2. While the absolute numerical confidence level is not known because the "correct" threshold is still somewhat arbitrary, the order of the connections, in terms of significance from greatest to least, is #4, #1, #2, and finally #3, which alone lacks some connecting density at the favored threshold.

Supplementary figures III-S3–S5 show sequence alignments for the three key motor proteins FliG, MotA, and MotB, which argue that their domain structure is conserved throughout bacteria. Though *Treponema primitia* strain ZAS-2 has not been sequenced, its 16S rRNA shares 86% and 85% sequence identity with that of *T. pallidum* and *T. denticola*, respectively. Thus the structural inferences about the positions, sizes, and interactions of their domains made here based on our *T. primitia* reconstruction are likely generally applicable. The organisms compared are the Gammaproteobacteria *E. coli* and *Salmonella typhimurium*; the Betaproteobacteria *Bordetella bronchiseptica*; the

Spirochetes *Treponema denticola*, *Treponema pallidum*, *Leptospira interrogans*, and *Borrelia burgdorferi*; the Firmicute *Bacillus subtilis*; *Thermotoga maritima*; the Epsilonproteobacteria *Helicobacter pylori*; the Deltaproteobacteria *Geobacter sulfurreducens*; and the Alphaproteobacteria *Agrobacterium tumefaciens*, except that in Fig. III-S3, *Agrobacterium tumefaciens* has been replaced with *Caulobacter crescentus*. Amino acids with 50% conservation are shaded in gray while those with 100% identity are shaded in black. The sequences were aligned with ClustalW[23] and presented using Alscript[24].

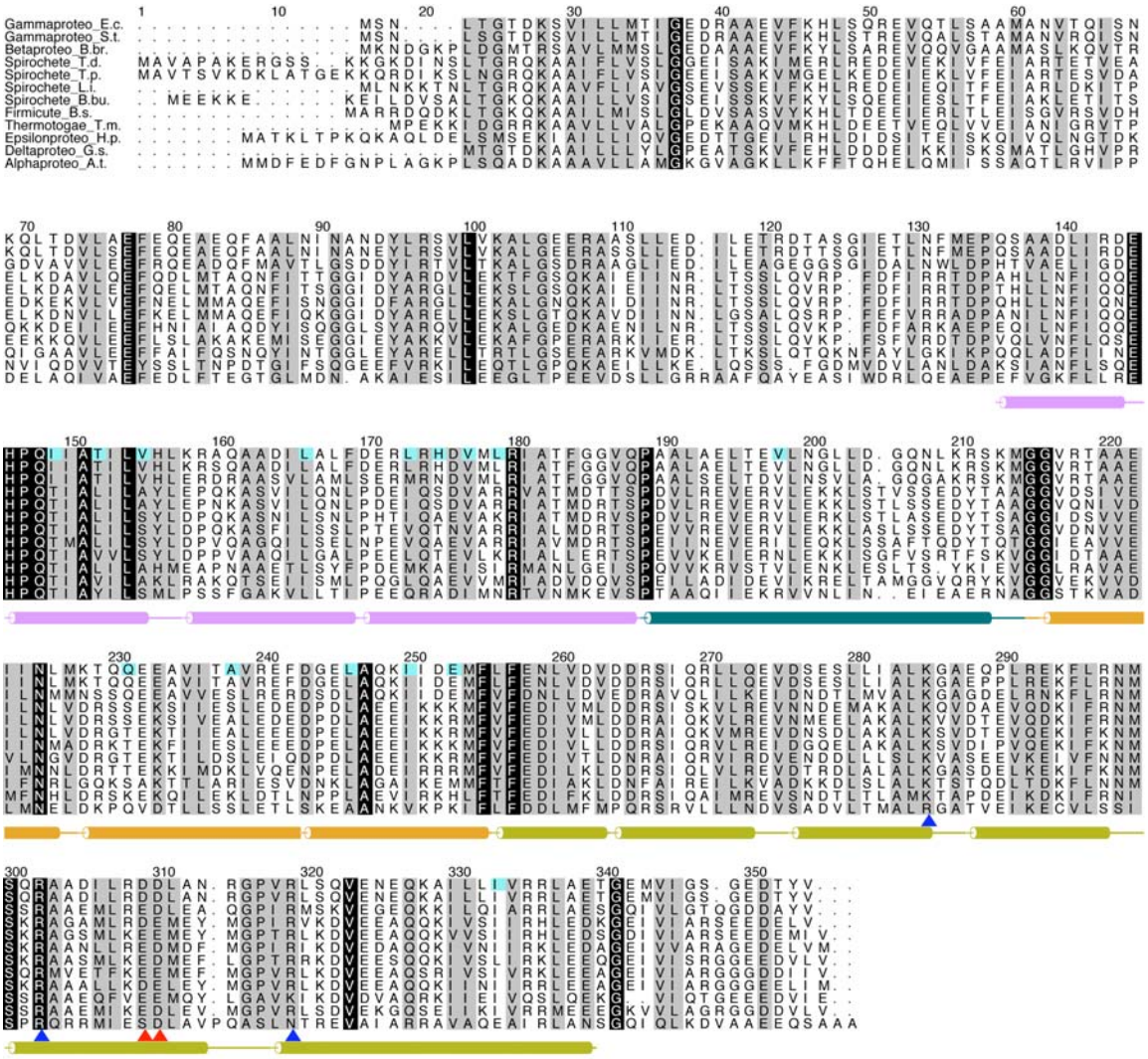

Figure III-S3. Sequence alignment of FliG.

The colored alpha-helices below the sequences are from the crystal structure of *T. maritima's* middle and C-terminal domains of FliG[19]. The pink region corresponds to the middle domain; the blue region corresponds to the 2 nm long helix that bridges the middle and C-terminal domains, and the orange and green regions correspond to the C-terminal domain. Amino acids shaded in cyan are those which, when mutated in *E. coli*, caused reduced binding to FliM in yeast 2-hybrid studies[25]. Notice they occur in both domains. The blue-colored and red-colored arrowheads are the conserved positively or

negatively charged amino acids that interact with the oppositely charged residues of MotA.[1]

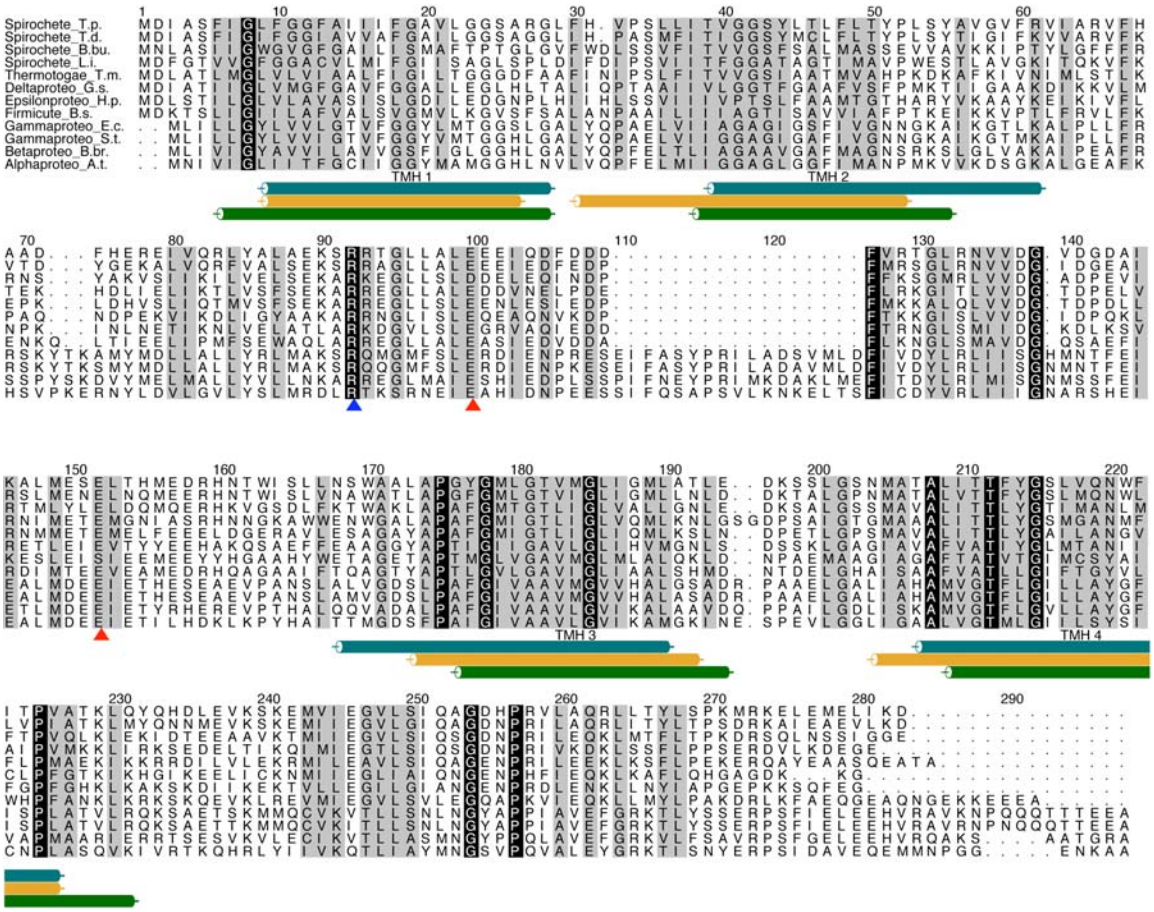

Figure III-S4. Sequence Alignment of MotA.

The colored helices correspond to the predicted transmembrane helices (TMH) generated by the TMHMM Server[26]. The blue helices correspond to the predicted helices of *T. pallidum*, the orange helices to *T. maritima*'s, and the green helices to *Salmonella*'s. The blue-colored and red-colored arrowheads are the conserved positively or negatively charged amino acids that interact with the oppositely charged residues of FliG.[1]

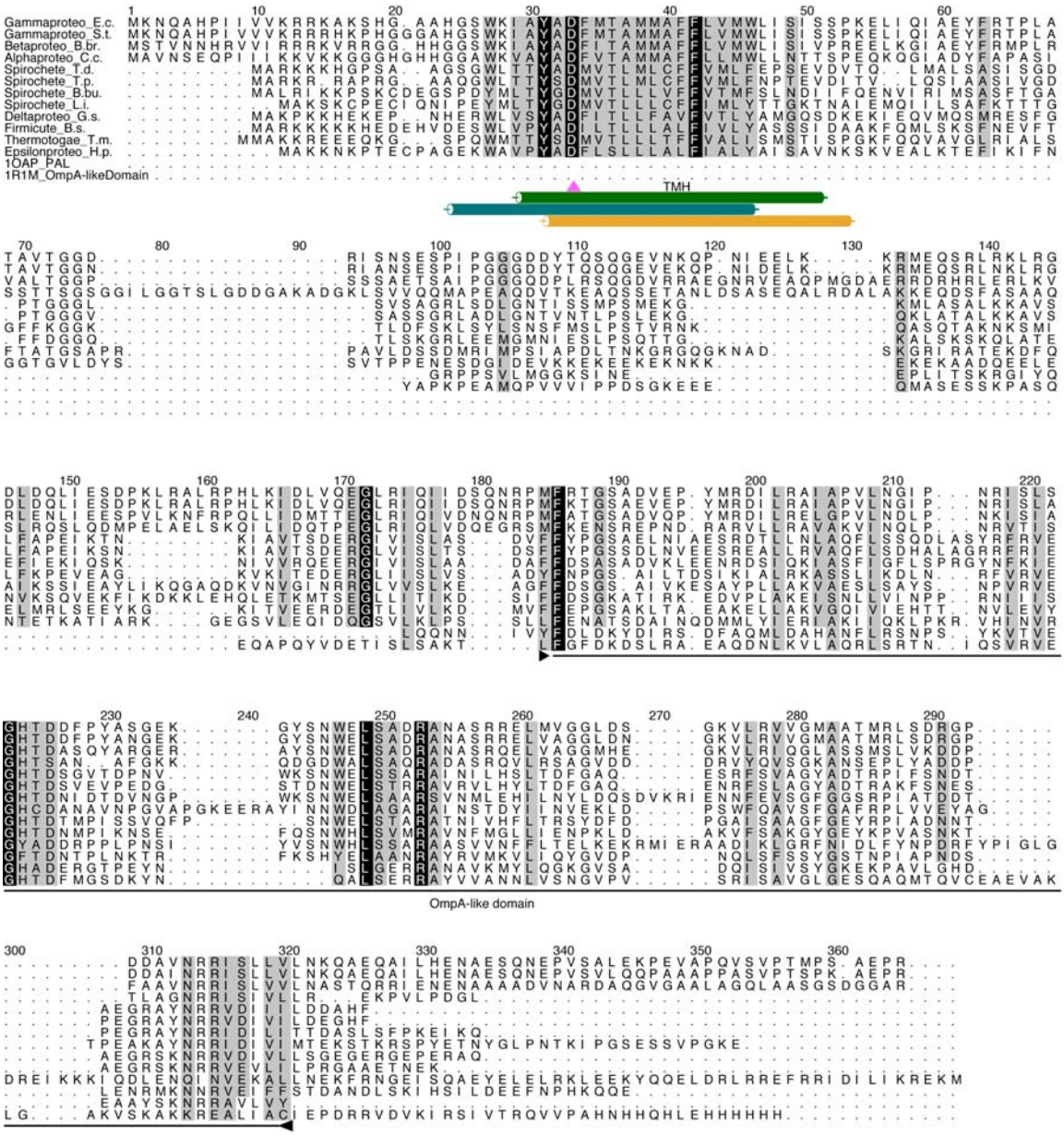

Figure III-S5. Sequence Alignment of MotB.

The colored helices are predicted and colored as in Figure III-S2. The pink arrowhead points to the conserved, protonatable aspartate residue.[1] The black line bounded by arrowheads delineates the OmpA-like domain that binds to the peptidoglycan layer. Also aligned are the chain sequences from the crystal structures of the *E. coli* Peptidoglycan-

associated lipoprotein (PDB id: 1OAP) and the OmpA-like domain from *N. meningitidis* RmpM (PDB id: 1R1M).

Supplementary Movie

The movie first shows orthoslices from top to bottom through the reconstruction of one *T. primitia* cell and then displays the segmented surfaces of tip filaments (green), the outer membrane (brown), the inner membrane (pink), the two periplasmic flagella (blue and red), and the surfaces of the motors for each flagella (blue and orange). An isosurface of the averaged, symmetrized flagellar motor is shown next (yellow), and finally the components that are thought to spin are colored in blue, while the fixed stator region is shown in yellow and orange.

Supplementary Methods

Cell Growth and Grid Preparation. Cultures were grown to an OD of ~ 0.6 at room temperature in sealed culture tubes containing 4YACo medium under a headspace of 80% H_2 and 20% CO_2 as described previously[21]. To prevent aggregation in high-salt solutions, 10 nm colloidal gold was pretreated with 5% BSA for 30 minutes. It was then concentrated five-fold and 5 ml was applied to glow-discharged, carbon-coated R 2/2 quantifoil grids, and then dried. Grids were plunge frozen in a Vitrobot (FEI Company) in 100% humidity.

Electron Tomography Data Collection and 3-D Reconstruction. Tilt series were acquired using the UCSF Tomo software[27]. Typically, tilts were incremented 1º from –63º to 63º. The magnification was 22,500 (0.98 nm/pixel) and the total dose was ~ 110 $e^-/Å^2$, distributed according to the 1/cos scheme. Tomograms were reconstructed using IMOD[28].

Image Processing. Bsoft[29] and the Peach distributed computing system[30] were used for image processing. Visualization and surface map measurements were done with Amira

(Mercury Computing Systems). The twenty extracted particles were bandpass-filtered between 200 nm and the first CTF zero. The missing wedge in reciprocal space was masked so that only measured regions of reciprocal space were used to align the particles, but no other object-specific mask was used. Course alignments were done in refine mode with an initial angular step size of 5° through all three Euler angles. Map averaging, symmetrization, and significance testing were done as described in the main text and supplementary figure legends.

Supplementary Notes

22. Frank, J. *Three-Dimensional Electron Microscopy of Macromolecular Assemblies* (Academic Press, San Diego, 1996).

23. Thompson, J. D., Higgins, D. G. & Gibson, T. J. CLUSTAL W: improving the sensitivity of progressive multiple sequence alignment through sequence weighting, position-specific gap penalties and weight matrix choice. *Nucleic Acids Res*. **22**, 4673-80 (1994).

24. Barton, G. J. ALSCRIPT: a tool to format multiple sequence alignments. *Protein Eng*. **6**, 37-40 (1993).

25. Marykwas, D. L. & Berg, H. C. A mutational analysis of the interaction between FliG and FliM, two components of the flagellar motor of *Escherichia coli*. *J. Bacteriol.* **178**, 1289-94 (1996).

26. Krogh, A., Larsson, B., von Heijne, G. & Sonnhammer, E. L. Predicting transmembrane protein topology with a hidden Markov model: application to complete genomes. *J. Mol. Biol.* **305**, 567-80 (2001).

27. Zheng, Q. S., Braunfeld, M. B., Sedat, J. W. & Agard, D. A. An improved strategy for automated electron microscopic tomography. *J. Struct. Biol.* **147**, 91-101 (2004).

28. Kremer, J. R., Mastronarde, D. N. & McIntosh, J. R. Computer visualization of three-dimensional image data using IMOD. *J. Struct. Biol.* **116**, 71-6 (1996).

29. Heymann, J. B. Bsoft: image and molecular processing in electron microscopy. *J. Struct. Biol.* **133**, 156-69 (2001).

30. Leong, P. A., Heymann, J. B. & Jensen, G. J. Peach: a simple Perl-based system for distributed computation and its application to cryo-EM data processing. *Structure* **13**, 505-11 (2005).